Structural predictions based on the compositions of cathodic materials by first-principles calculations

Yang Li[1), Fang Lian[1), Ning Chen[1), Zhen-jia Hao[1), and Kuo-chih Chou[1,2)

1) School of Materials Science and Engineering, University of Science and Technology Beijing, Beijing 100083, China

2) School of Metallurgical and Ecological Engineering, University of Science and Technology Beijing, Beijing 100083, China

Abstract: A first-principles method is applied to comparatively study the stability of lithium metal oxides with layered or spinel structures to predict the most energetically favorable structure for different compositions. The binding and reaction energies of the real or virtual layered $LiMO_2$ and spinel LiM_2O_4 (M = Sc–Cu, Y–Ag, Mg–Sr, and Al–In) are calculated. The effect of element M on the structural stability, especially in the case of multiple-cation compounds, is discussed herein. The calculation results indicate that the phase stability depends on both the binding and reaction energies. The oxidation state of element M also plays a role in determining the dominant structure, i.e., layered or spinel phase. Moreover, calculation-based theoretical predictions of the phase stability of the doped materials agree with the previously reported experimental data.

Keywords: lithium-ion batteries; cathodic materials; structure; first-principles calculations; binding energy

1. Introduction

Lithium-ion batteries (LIBs) are acknowledged as one of the most important technologies for electrical energy storage because of their high energy density. The performance of LIBs critically depends on the intrinsic properties of their electrode materials. The design and application of novel cathode materials will enable significant improvements in the performance of LIBs [1–3]. Generally, LIB active cathode materials are lithium-intercalation oxides [4–5], which are structurally classified as layered (e.g., $LiCoO_2$), spinel (e.g., $LiMn_2O_4$), or olivine (e.g., $LiFePO_4$) phases [6]. Computation could be the most powerful complementarity for experiments, which is beneficial for understanding macro-properties and designing novel materials [7–8]. First-principles calculations based on the density functional theory (DFT) to solve the Schrödinger equation under some rational approximations have been applied to calculate the average lithium intercalation voltage [9–10], analyze the Li^+ intercalation and deintercalation mechanism [11–12], and optimize the structure [13–15] of LIB electrode materials.

The presence of spinel-like structures in the as-prepared layered materials and the gradual transformation of layered compounds into spinel-like structures during cycling are well known to result in capacity fading, stability deterioration, and safety problems in LIBs [16–17]. Such phase transformations have been investigated via theoretical studies, most of which have been focused on the influence of the Li concentration in the cathode material during electrochemical cycling [18]. Doping is known to be an effective experimental approach to tailoring LIB cathode materials; this approach can improve the materials' structural stability and electrochemical performance. Therefore, understanding the influence of doping on the structural properties of cathode materials through calculations is an effective way to determine the dopants and dopant concentrations that will result in cathode materials with excellent electrochemical properties

In this work, we modeled the real or virtual layered ($LiMO_2$) and spinel (LiM_2O_4) phases with their M-sites occupied by 4th- and 5th-period transition metals and some of the 2nd- and 3rd-subgroup metals; we also calculated binding energies of two phases and the reaction energies of lay-

                                                          Springer

ered phases [19]. This study was focused on the stability of specific compounds and on the influence of different metals or dopants in the M-sites on the structural stability of layered cathode materials.

2. Methods

2.1. First-principles methodology

First-principles calculations were performed using the Cambridge Sequential Total Energy Package (CASTEP) [20], which is based on DFT. The exchange-correlation potential was described by the spin-polarized generalized gradient approximation (GGA) as implemented in the PW91 functional [21]. The calculations were performed via ultrasoft pseudopotential plane-wave bases with an energy cutoff value of 380 eV. The GGA+U method was performed to mitigate the self-interaction error in calculating the materials with 4th-and 5th-period transition metals that contain localized d electrons. The U-values were chosen to be 3.5 for the 4th-period and 2.5 for the 5th-period transition metals. All of the metal elements were set to be in their high-spin state and in the up direction. Additionally, a k-mesh of $10 \times 10 \times 10$ for layered phases and $5 \times 5 \times 5$ for spinel phases over the Brillouin zone were used.

In the calculations, the conjugate gradient minimization (CG) method was selected for electronic energy minimiza-

tion. The Pulay density-mixing scheme was used in the computations of self-consistent total energy. The self-consistent field tolerance was set as 5×10^{-7} eV/atom. Moreover, lattice parameters and atomic positions were relaxed according to the Broyden–Fletcher–Goldfarb–Shanno (BFGS) scheme to minimize the total energy. The optimization procedure was terminated when the total energy converged to 5×10^{-6} eV/atom and the residual force was less than 0.1 eV/nm. The atomic displacement and the stress converged to 5×10^{-5} nm and 2×10^{7} Pa, respectively.
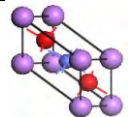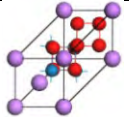
2.2. Calculation models

The lattice models were first constructed on the basis of the crystal parameters of $LiCoO_2$ and $LiMn_2O_4$ to describe layered and spinel phases, respectively, as shown in Table 1 and Table 2. Subsequently, geometry optimizations for the real or virtual phases with M replaced by other transition-metal elements in the 4th and 5th periods or by some metals in the 2nd and 3rd subgroups were performed during the calculation process.

Table 1. Lattice parameters of $LiCoO_2$ and $LiMn_2O_4$

Materials	Space group	a / nm	b / nm	c / nm
$LiCoO_2$	$R\bar{3}m$	0.28160	0.28160	1.40510
$LiMn_2O_4$	$Fd\bar{3}m$	0.82487	0.82487	0.82487

Table 2. Structure models and atom positional parameters of $LiCoO_2$ and $LiMn_2O_4$

Layered-$LiCoO_2$					Spinel-$LiMn_2O_4$				
Crystal model	Atom(site)	x	y	z	Crystal model	Atom(site)	x	y	z
	Li(3a)	0	0	0		Li(8a)	0	0	0
	Co(3b)	0	0	0.500		Mn(16d)	0.375	0.375	0.375
	O(6c)	0	0	0.260		O(32e)	0.388	0.388	0.388

3. Results and discussion

3.1. Binding energy E_B and reaction energies E_R

The total energy of a system is generally obtained from energy calculations, which unfortunately cannot represent the structural stability of a material directly. In the present work, binding energies were calculated as fundamental data for predicting the phase stability of materials [22–23].

The binding energy E_B is given by the following expression:

$$E_B = \sum E_{\text{Atom}(k)} n_{(k)} - E_{\text{Total}} \tag{1}$$

where E_{Total} is the total energy of the crystal lattice, $E_{\text{Atom}(k)}$ is the total energy of isolated atom k in vacuum, and $n_{(k)}$ is

the number of atom k. In addition, a $1 \times 1 \times 1$ nm^3 supercell ($P1$ space group) with isolated atom k in the center was constructed to calculate $E_{\text{Atom}(k)}$ [22]. E_B is related to the phase stability of the material: a larger E_B indicates that the structure is more likely to exist and be stable in reality.

The structural evolution reaction from layered-phase $LiMO_2$ to spinel-phase LiM_2O_4 can be expressed as

$$LiMO_2 + \frac{1}{8}O_2 = \frac{1}{2}LiM_2O_4 + \frac{1}{4}Li_2O \tag{2}$$
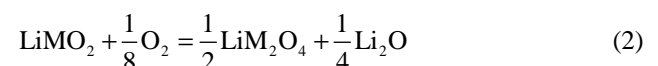
This structural evolution originates from the rearrangement of Li^+ and transition-metal M ions, which corresponds to the variance in the number of atoms of the calculation model. In view of the difference in atomic ratios between $LiMO_2$ and LiM_2O_4, the binding energy of spinel-phase LiM_2O_4 is rep-

526

Int. J. Miner. Metall. Mater., Vol. 22, No. 5, May 2015

resented as $[E_B(LiM_2O_4) + 1/2E_B(Li_2O) - 1/4E_B(O_2)]/2$ in comparison to that of layered $LiMO_2$. Therefore, the difference in binding energies between layered-phase $LiMO_2$ and spinel-phase LiM_2O_4 can be described as $E_B(LiMO_2) - [E_B(LiM_2O_4) + 1/2E_B(Li_2O) - 1/4E_B(O_2)]/2$, which is numerically equal to $E_{Total}(LiMO_2) - [E_{Total}(LiM_2O_4) + 1/2E_{Total}(Li_2O) - 1/4E_{Total}(O_2)]/2$ and to the ΔG of the structural evolution reaction (2). More importantly, binding energies E_B in the calculation replace E_{Total}, which is physically meaningless without any energy reference. Therefore, the stability difference between layered-phase $LiMO_2$ and spinel-phase LiM_2O_4 was described according to the difference in E_B, which is expressed as $E_B(LiMO_2) - [E_B(LiM_2O_4) + 1/2E_B(Li_2O) - 1/4E_B(O_2)]/2$.

Li$_2$O and O$_2$ were calculated as illustrated in the preceding section (as described in 2.1 First-principles methodology). The lattice parameters of Li_2O were $a = b = c = 0.32994$ nm, and Li and O occupied positions $(0.25, 0.25, 0.25)$ and $(0.5, 0.5, 0.5)$, respectively. The structure of O_2 was constructed in a $1 \times 1 \times 1$ nm^3 supercell, and the two oxygen atoms occupied positions $(1, 0, 0)$ and $(1, 1.3, 0)$, respectively. Because the distance between each oxygen molecule in the supercell was sufficiently large, the oxygen molecules were considered to be isolated from each other. Thus, the calculated energy could be approximated as the free oxygen molecule energy. The variation tendencies of the binding energy E_B as functions of element M in layered $LiMO_2$ and in spinel LiM_2O_4 are shown in Fig. 1.
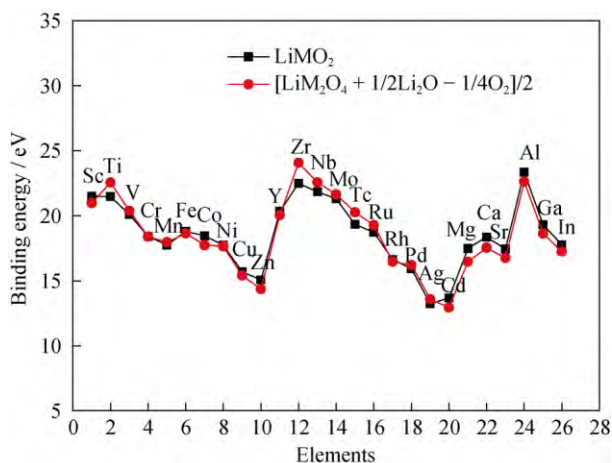

Fig. 1. Comparison between the binding energies of the corresponding real or virtual phases (M = transition-metal elements in the 4th and 5th periods and some elements in the 2nd and 3rd subgroups).

In addition, reaction energies E_R were also calculated; these energies are described as the difference of the sum of the binding energy between products and reactants. In the present work, E_R was combined with the binding energy E_B to precisely predict the phase stability of a material. E_R is represented by

$$E_R = \sum E_B(\text{Reactant}) - \sum E_B(\text{Product}) \qquad (3)$$

The formation reaction of layered-phase $LiMO_2$ from Li_2O, O_2, and the M-oxide $MO_{x/2}$ ($x = 1$–5; the oxidation state of element M refers to that in the most stable M-oxide) is represented as

$$\frac{1}{2}Li_2O + MO_{x/2} + \frac{3-x}{4}O_2 = LiMO_2 \qquad (4)$$
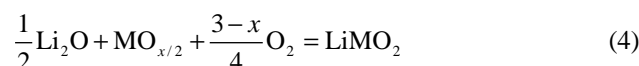
Thus, the reaction energy E_R can be expressed as

$$E_R(4) = E_B(MO_{x/2}) + \frac{1}{2}E_B(Li_2O) +$$
$$\frac{3-x}{4}E_B(O_2) - E_B(LiMO_2) \qquad (5)$$

The energies of the M-oxides were calculated as illustrated in the preceding section (2.1 First-principles methodology). E_R determines the driving force of a formation reaction; i.e., a reaction with a greater E_R will be more likely to occur to form the more stable product.

3.2. Prediction of dominant phase between layered LiMO$_2$ and spinel LiM$_2$O$_4$

The dominant-phase figure of real and virtual phases was plotted on the basis of the calculated results of E_B and E_R, as shown in Fig. 2. In this figure, the Y-axis represents the difference in E_B values between the layered $LiMO_2$ and spinel LiM_2O_4 phases (based on Fig. 1), which reduces the partial influence of the system error induced from the selection of calculation parameters such as the exchange-correlation functional, U values, calculation model, crystal constant, etc. The X-axis depicts the reaction energy E_R of the layered phase. The plot can be divided into three dominant regions: a layered stable region, a spinel stable region, and an unstable region, which indicates clearly the energetically favorable phases with different elements M. The negative X-values in Fig. 2 suggest that systems with elements M such as Zr, Ti, and Ru in the unstable region cannot exist as stable layered phases [24]. Additionally, a larger value of X indicates a larger E_R, implying that the compound is inclined to be synthesized or to be stable in reality. The system with M = Co and Ni appears in the layered stable region, whereas the system with M = Mn locates in the spinel stable region. The calculation results confirm that, unlike Co and Ni, Mn does not form a stable layered $LiMnO_2$ phase. The system with M = Mn prefers the spinel structure rather than the layered one. In addition, the positive X-value of M = Co, Ni, and Mn indicates that a layered phase containing these three

elements can be synthesized in reality. However, layered $LiMnO_2$ is much more difficult to prepare and suffers a severe structural transformation to the spinel phase during the charge/discharge process. Similarly, the absolute value of the *Y*-axis value for M = Co is much larger than that for M = Ni, whose *Y*-value lies very close to the *X*-axis (i.e., it lies close to *Y* = 0), which suggests that layered $LiCoO_2$ is more stable than layered $LiNiO_2$ [2,7]. Furthermore, the results related to the large *X*-value of M = Fe in Fig. 2 predict that the synthesis of layered $LiFeO_2$ is easy, consistent with reported experimental observations [25]. Likewise, the calculation results indicate that layered $LiVO_2$ is not stable, consistent with this material's reported irreversible transformation to the spinel phase during delithiation [26].
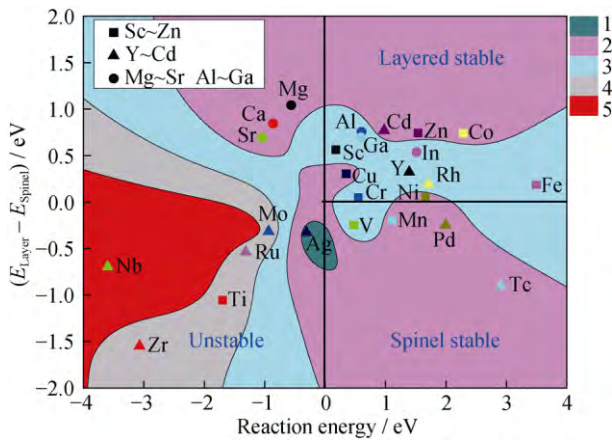

Fig. 2. Distribution of the calculated phases for layered and spinel structures (M= transition metal elements in the 4th and 5th periods, and some elements in the 2nd and 3rd subgroups). The shaded areas distinguish the difference in the valence of a given element M: green, pink, blue, gray, and red indicate valences of 1+, 2+, 3+, 4+, and 5+, respectively.

In addition, the areas in Fig. 2 are marked in different colors according to the common oxidation state of the element M (i.e., a valence of 1+, 2+, 3+, 4+, or 5+). The stability of the dominant phase is closely related to the oxidation state of element M. Elements M in 4+ or 5+ valence states lie almost in the unstable region. For example, the smaller *X*-value of the Nb system with a 5+ valence element demonstrates that layered $LiNbO_2$ is very difficult to synthesize in reality. In contrast, elements M in 2+ and 3+ valence states occupy the region of *X* > 0 in the dominant-phase figure; additionally, elements M in a 3+ valence state almost all locate in the layered stable region, which indicates that a layered phase with M in the 3+ valence is likely to be more stable. We concluded from the color contours that layered phases with elements M in high valence states (4+ or 5+) are clearly difficult to prepare and less stable but that layered phases with most of the elements M in 2+ or 3+ valence states can be synthesized; in particular, phases with M^{3+} tend to be stable.

The coexistence of several elements M in layered $LiMO_2$, such as phases prepared via multiple-cation doping, appears to be an effective method to improve the stability of $LiMO_2$. The partial substitution of Ni in $LiNiO_2$ by one or more metal ions such as Co, Al, Mn, Ga, Mg, and Ti has previously been proposed and investigated [2,27–29]. Some reported layered-structure compounds with multiple cations are included in Table 3. The crystal structure affects the diffusion pathway for Li^+ and the diffusion coefficient of Li^+ (D_{Li+}) in cathode materials [30]. For example, 2D layered $LiCoO_2$ exhibits greater Li^+ diffusivity than 3D spinel $LiMn_2O_4$ [31]. Thus, reported D_{Li+} values of compounds with multiple cations are also included in Table 3 to reveal the relationship between our calculation results, i.e., the dominant-phase figure, and the macro-performances of cathode materials. To ensure comparability of the results from different references, only D_{Li+} data determined by the galvanostatic intermittent titration technique (GITT) were selected. Supposing that the binding energy of these multiple phases can be linearly superimposed on each other, the

Table 3.   Typical layered cathode materials and their lithium diffusion coefficients

Number	Formula	B-site elements	Diffusion coefficient / $(10^{-16}\ m^2 \cdot s^{-1})$	Reference
1	$LiCoO_2$	Co	500	[32–33]
2	$LiNi_{0.15}Co_{0.85}O_2$	Ni, Co	300	[34]
3	$LiCo_{0.75}Al_{0.25}O_2$	Co, Al	120	[35]
4	$LiCo_{0.6}Ni_{0.4}O_2$	Co, Ni	100	[36]
5	$LiCo_{0.5}Ni_{0.5}O_2$	Co, Ni	90	[37]
6	$LiNi_{0.75}Co_{0.2}Mg_{0.05}O_2$	Ni, Co, Mg	30	[38]
7	$LiNi_{0.5}Mn_{0.3}Co_{0.2}O_2$	Ni, Mn, Co	19	[39]
8	$LiMn_{0.4}Ni_{0.4}Co_{0.2}O_2$	Mn, Ni, Co	13.87	[40]
9	$LiNi_{0.75}Al_{0.25}O_2$	Ni, Al	4	[41]
10	$LiNiO_2$	Ni	1	[41]

location of these reported multiple M compounds can be determined in the dominant-phase figure (Fig. 2) via the ingredient percentage weighted average method, as shown in Fig. 3. For example, the values of X and Y for $LiNi_{0.75}Co_{0.2}Mg_{0.05}O_2$ (the 6th compound) in Fig. 3 can be calculated from the formulae $X = 0.75X_{Ni} + 0.2X_{Co} + 0.05X_{Mg}$ and $Y = 0.75Y_{Ni} + 0.2Y_{Co} + 0.05Y_{Mg}$, respectively. The definite location of a compound with multiple cations can predict its stability; specifically, larger values of X and/or Y predict a more stable layered structure and a relatively greater D_{Li+} value for multiple-cation compounds, which is consistent with the experimental data reported in the literature (listed in Table 3). Therefore, we conclude that the dominant-phase figure derived from the first-principles calculations is a powerful tool to predict the effect of doping on the structural stability of layered cathode materials.
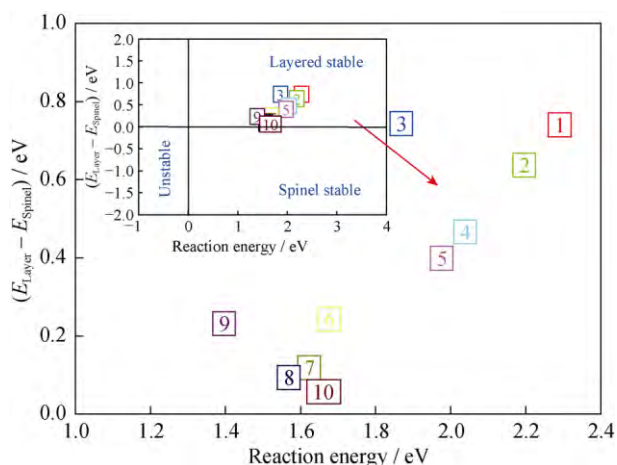

Fig. 3. Location of the reported $LiMO_2$ layered materials (Table 3) in a dominant-phase figure. The X and Y values were calculated in terms of related component proportion.

4. Conclusions

(1) The structural stability between the layered $LiMO_2$ and spinel LiM_2O_4 (M = Sc–Cu, Y–Ag, Mg–Sr, and Al–In) and the influence of M as dopants on the preferential phase were studied by comparing the binding and reaction energies determined via the first-principles calculations.

(2) A dominant-phase figure was obtained on the basis of the calculation results for the binding energies of two phases and the reaction energies of layered phases; the results indicate that the dominant phase between layered $LiMO_2$ and spinel LiM_2O_4 is closely related to the oxidation state of element M.

(3) The location of the compounds with multiple M cations in the dominant-phase figure was determined by the

ingredient percentage weighted average method. The theoretically predicted phase stabilities and Li^+ diffusion coefficients of multiple-cation materials are in agreement with the previously reported experimental data. Thus, the dominant-phase figure offers a reliable route to the effective design of novel LIB cathode materials.

Acknowledgements

References

[1] M.S. Whittingham, Lithium batteries and cathode materials, *Chem. Rev.*, 104(2004), No. 10, p. 4271.

[2] P. He, H.J. Yu, D. Li, and H.S. Zhou, Layered lithium transition metal oxide cathodes towards high energy lithium-ion batteries, *J. Mater. Chem.*, 22(2012), p. 3680.

[3] M.M. Thackeray, C. Wolverton, and E.D. Isaacs, Electrical energy storage for transportation-approaching the limits of, and going beyond, lithium-ion batteries, *Energy Environ. Sci.*, 5(2012), p. 7854.

[4] G. Ceder, G. Hautier, A. Jain, and S.P. Ong, Recharging lithium battery research with first-principles methods, *MRS Bull.*, 36(2011), No. 3, p. 185.

[5] G. Ceder and M.K. Aydinol, The electrochemical stability of lithium–metal oxides against metal reduction, *Solid State Ionics*, 109(1998), No. 1-2, p. 151.

[6] B. Xu, D.N. Qian, Z.Y. Wang, and Y.S. Meng, Recent progress in cathode materials research for advanced lithium ion batteries, *Mater. Sci. Eng. R*, 73(2012), No. 5-6, p. 51.

[7] J.J. Saavedra-Arias, C.V. Rao, J. Shojan, A. Manivannan, L. Torres, Y. Ishikawa, and R.S. Katiyar, A combined first-principles computational/experimental study on $LiNi_{0.66}Co_{0.17}Mn_{0.17}O_2$ as a potential layered cathode material, *J. Power Sources*, 211(2012), p. 12.

[8] A. Jain, G. Hautier, C.J. Moore, S. Ping Ong, C.C. Fischer, T. Mueller, K.A. Persson, and G. Ceder, A high-throughput infrastructure for density functional theory calculations, *Comput. Mater. Sci.*, 50(2011), No. 8, p. 2295.

[9] M.K. Aydinol, A.F. Kohan, and G. Ceder, *Ab initio* calculation of the intercalation voltage of lithium–transition-metal oxide electrodes for rechargeable batteries, *J. Power. Sources*, 68(1997), No. 2, p. 664.

[10] L. Benco, J.L. Barras, M. Atanasov, C.A. Daul, and E. Deiss, First-principles prediction of voltages of lithiated oxides for lithium-ion batteries, *Solid State Ionics*, 112(1998), No. 3-4, p. 255.

[11] Z.F. Huang, H.Z. Zhang, C.Z. Wang, D.P. Wang, X. Meng, M. Xing, and G. Chen, First-principles investigation on extraction of lithium ion from monoclinic $LiMnO_2$, *Solid State*

Sci., 11(2009), No. 1, p. 271.

[12] A. Van der Ven and G. Ceder, Lithium diffusion mechanisms in layered intercalation compounds, *J. Power Sources*, 97-98(2001), p. 529.

[13] S.K. Mishra and G. Ceder, Structural stability of lithium manganese oxides, *Phys. Rev. B*, 59(1999), No. 9, p. 6120.

[14] M. Nakayama and M. Nogami, A first-principles study on phase transition induced by charge ordering of Mn^{3+}/Mn^{4+} in spinel $LiMn_2O_4$, *Solid State Commun.*, 150(2010), No. 29-30, p. 1329.

[15] M.E. Arroyo y de Dompablo and G. Ceder, First-principles calculations on Li_xNiO_2: phase stability and monoclinic distortion, *J. Power Sources*, 119-121(2003), p. 654.

[16] A.R. Armstrong, A.J. Paterson, N. Dupré, C.P. Grey, and P.G. Bruce, Structural evolution of layered $Li_xMn_yO_2$ combined neutron, NMR, and electrochemical study, *Chem. Mater.*, 19(2007), No. 5, p. 1016.

[17] F. Capitaine, P. Gravereau, and C. Delmas, A new variety of $LiMnO_2$ with a layered structure, *Solid State Ionics*, 89(1996), No. 3-4, p. 197.

[18] J. Reed and G. Ceder, Role of electronic structure in the susceptibility of metastable transition-metal oxide structures to transformation, *Chem. Rev.*, 104(2004), No. 10, p. 4513.

[19] N. Li, N. Chen, F.S. Li, Y. Li, and H.L. Zhao, Theoretical research on optimization ingredient regulation of $BaBO_3$ series hypoxic materials, *Sci. China Phys. Mech. Astron.*, 41(2011), No. 9, p. 1075.

[20] M.D. Segall, P.J.D. Lindan, M.J. Probert, C.J. Pickard, P.J. Hasnip, S.J. Clark, and M.C. Payne, First-principles simulation: ideas, illustrations and the CASTEP code, *J. Phys. Condens. Matter*, 14(2002), No. 11, p. 2717.

[21] Y. Wang and J.P. Perdew, Correlation hole of the spin-polarized electron gas, with exact small-wave-vector and high-density scaling, *Phys. Rev. B*, 44(1991), No. 24, p. 13298.

[22] D.W. Zhou, J.S. Liu, S.H. Xu, and P. Peng, First-principles investigation of the binary intermetallics in Mg–Al–Sr alloy: stability, elastic properties and electronic structure, *Comput. Mater. Sci.*, 86(2014), p. 24.

[23] X. Chong, Y. Jiang, R. Zhou, and J. Feng, First principles study the stability, mechanical and electronic properties of manganese carbides, *Comput. Mater. Sci.*, 87(2014), p. 19.

[24] R. Koksbang, J. Barker, H. Shi, and M.Y. Saïdi, Cathode materials for lithium rocking chair batteries, *Solid State Ionics*, 84(1996), No. 1-2, p. 1.

[25] T. Shirane, R. Kanno, Y. Kawamoto, Y. Takeda, M. Takano, T. Kamiyama, and F. Izumi, Structure and physical properties of lithium iron oxide, $LiFeO_2$, synthesized by ionic exchange reaction, *Solid State Ionics*, 79(1995), p. 227.

[26] L.A. de Picciotto and M.M. Thackeray, Transformation of delithiated $LiVO_2$ to the spinel structure, *Mater. Res. Bull.*, 20(1985), No. 2, p. 187.

[27] T. Ohzuku and Y. Makimura, Layered lithium insertion material of $LiCo_{1/3}Ni_{1/3}Mn_{1/3}O_2$ for lithium-ion batteries, *Chem. Lett.*, 30(2001), No. 7, p. 642.

[28] T. Ohzuku, T. Yanagawa, M. Kouguchi, and A. Ueda, Innovative insertion material of $LiAl_{1/4}Ni_{3/4}O_2$ ($R\overline{3}m$) for lithium-ion (shuttlecock) batteries, *J. Power Sources*, 68(1997), No. 1, p. 131.

[29] R. Sathiyamoorthi, P. Santhosh, P. Shakkthivel, and T. Vasudevan, $LiNi_{0.8}Co_{0.2-x}Ti_xO_2$ nanoparticles: synthesis, structure, and evaluation of electrochemical properties for lithium ion cell application, *J. Solid State Electrochem.*, 11(2007), p. 1665.

[30] E. Deiss, Spurious chemical diffusion coefficients of Li^+ in electrode materials evaluated with GITT, *Electrochim. Acta*, 50(2005), No. 14, p. 2927.

[31] M. Park, X. Zhang, M. Chung, G.B. Less, and A.M. Sastry, A review of conduction phenomena in Li-ion batteries, *J. Power Sources*, 195(2010), No. 24, p. 7904.

[32] Y.M. Choi and S.I. Pyun, Determination of electrochemical active area of porous $Li_{1-\delta}CoO_2$ electrode using the GITT technique, *Solid State Ionics*, 109(1998), No. 1-2, p. 159.

[33] H.W. Yan, X.J. Huang, H. Li, and L.Q. Chen, Electrochemical study on $LiCoO_2$ synthesized by microwave energy, *Solid State Ionics*, 113-115(1998), p. 11.

[34] J. Molenda, P. Wilk, and J. Marzec, Electronic and electrochemical properties of $Li_xNi_{1-y}Co_yO_2$ cathode material, *Solid State Ionics*, 157(2003), No. 1-4, p. 115.

[35] C. Julien, M.A. Camacho-Lopez, M. Lemal, and S. Ziolkiewicz, $LiCo_{1-y}M_yO_2$ positive electrodes for rechargeable lithium batteries: I. Aluminum doped materials, *Mater. Sci. Eng. B*, 95(2002), No. 1, p. 6.

[36] C.M. Julien, A. Amdouni, S. Castro-Garcia, M. Selmane, and S. Rangan, $LiCo_{1-y}M_yO_2$ positive electrodes for rechargeable lithium batteries: II. Nickel substituted materials grown by the citrate method, *Mater. Sci. Eng. B*, 128(2006), No. 1-3, p. 138.

[37] L.A. Montoro and J.M. Rosolen, The role of structural and electronic alterations on the lithium diffusion in $Li_xCo_{0.5}Ni_{0.5}O_2$, *Electrochim. Acta*, 49(2004), No. 19, p. 3243.

[38] Y.D. Zhong, X.B. Zhao, and G.S. Cao, Characterization of solid-state synthesized pure and doped lithium nickel cobalt oxides, *Mater. Sci. Eng. B*, 121(2005), No. 3, p. 248.

[39] S.Y. Yang, X.Y. Wang, X.K. Yang, Y.S. Bai, Z.L. Liu, H.B. Shu, and Q.L. Wei, Determination of the chemical diffusion coefficient of lithium ions in spherical $Li[Ni_{0.5}Mn_{0.3}Co_{0.2}]O_2$, *Electrochim. Acta*, 66(2012), p. 88.

[40] S.J. Shi, Y.J. Mai, Y.Y. Tang, C.D. Gu, X.L. Wang, and J.P. Tu, Preparation and electrochemical performance of ball-like $LiMn_{0.4}Ni_{0.4}Co_{0.2}O_2$ cathode materials, *Electrochim. Acta*, 77(2012), p. 39.

[41] G.X. Wang, S. Zhong, D.H. Bradhurst, S.X. Dou, and H.K. Liu, $LiAl_{\delta}Ni_{1-\delta}O_2$ solid solutions as cathodic materials for rechargeable lithium batteries, *Solid State Ionics*, 116(1999), No. 3-4, p. 271.